

Effects of step–step interactions on the fluctuations of an individual step on a vicinal surface and its wavelength dependence

Hyeong-Chai Jeong ^{a,*}, John D. Weeks ^b

^a Department of Physics, Sejong University, Kwangjin-Ku, Seoul 143-747, South Korea

^b Institute for Physical Science and Technology and Department of Chemistry, University of Maryland, College Park, MD 20742, USA

Received 9 November 1998; accepted for publication 13 April 1999

Abstract

We relate properties of an anisotropic continuum model of a two-dimensional vicinal surface to those of a model with fluctuating and interacting steps. We show that analysis of the fluctuations of an *individual* step in the array provides information about the length scale on which the surface has reached equilibrium and can be used to estimate fundamental step parameters from locally equilibrated surfaces. Monte Carlo simulations of a stable vicinal surface using the terrace–step–kink model agree with the theoretical predictions. We further apply this analysis to steps on an *unstable* surface during reconstruction-induced faceting and show that it can be used to determine whether the faceting process is in the nucleation or spinodal decomposition regime. © 1999 Elsevier Science B.V. All rights reserved.

Keywords: Capillary waves; Faceting; Fluctuation; Step; Surface kinetics; Surface thermodynamics; Vicinal surface

1. Introduction

Steps play an essential role in determining the structure of crystal surfaces at low temperatures and in many surface kinetic processes. Thus the evolution of surface morphology has often been characterized in terms of models describing the motion of individual steps [1,2]. Direct imaging techniques, such as scanning tunneling microscopy (STM), reflection electron microscopy (REM) and low-energy electron microscopy (LEEM), allow us to observe individual step configurations and determine their motion quantitatively.

Important theoretical insight has arisen from a capillary wave analysis [3,4] of the fluctuations of

steps on vicinal surfaces combined with exact solutions of the free-fermion model [5–10]. In particular, Yamamoto and coworkers [9,11,12] studied the mean-squared fluctuation width of an individual step on a vicinal surface and showed that it exhibits an asymptotic logarithmic behavior, in contrast to the linear behavior of a single isolated step (see below for precise definitions). They pointed out that a key macroscopic parameter in the step model, the *step interaction strength*, could in principle be determined by fitting experimental data to the predicted logarithmic form. Indeed, this and other fundamental parameters in the step model, such as the *step stiffness* and the *step mobility*, have been estimated from experimental data on the mean-square step displacements [5–9], and the distribution of terrace widths [13,14].

* Corresponding author. Fax: +82-2-3408-3569.

E-mail address: hcj@kunjja.sejong.ac.kr (H.-C. Jeong)

However, well-equilibrated surface step configurations are needed to obtain accurate parameter values from the terrace width distribution and mean-square step displacements, while we are often interested in the properties of surfaces under dynamical conditions where the surface structure has reached *local* equilibrium but the long wavelength modes may not have completely relaxed. In this paper, we show that it is still possible to determine accurate parameter values in many such cases by analyzing how the Fourier modes of the fluctuations of an individual step on the vicinal surface differ from those of a single isolated step. This provides a sensitive probe of the effects of step–step interactions on a variety of different length scales. Our approach yields an estimate of the length scale on which a real surface has reached equilibrium and can be used to determine the basic step parameters.

In the following sections, we first analyze the equilibrium fluctuations of an individual step on a uniform stable vicinal surface [9,11,12]. By comparing this to the fluctuations of a single isolated step, we develop a method for subtracting the effects of step–step interactions from the wavelength dependence of the fluctuation modes of the step. This allows us to determine the interaction strength and other parameters. Monte Carlo simulations using the terrace–step–kink (TSK) model confirm the accuracy of these predictions. We then apply this same analysis to the steps on an *unstable* vicinal surface undergoing reconstruction-driven faceting and show that it can determine whether the surface is in the nucleation or spinodal decomposition regime.

2. Capillary waves and energetic parameters for the step Hamiltonian

On an atomic scale, the fluctuations of individual steps are controlled by the microscopic energy cost to form kinks. In the following we operate on a coarse grained mesoscopic scale, where atomic scale fluctuations like kinks cannot be resolved. The individual surface steps are treated as the fundamental objects of interest and mass transport between them is explicitly considered. In this model

a step can be pictured as a continuous fluctuating line or string with an effective line tension or *step stiffness*, $\tilde{\beta}$, that tends to keep the step straight. The energy of small long wavelength distortions of a single *isolated* fluctuating step can be simply written as:

$$H = \frac{1}{2} \int \tilde{\beta} [\partial_y x(y)]^2 dy \quad (1)$$

where the y -direction is set to the step-edge direction and $x(y)$ represents the configuration of the step. We refer to this quadratic Hamiltonian as a capillary wave model in analogy to the capillary wave model of the liquid–vapor interface [3,4]. It can be diagonalized by a Fourier transform: $H = \frac{1}{2} \tilde{\beta} \sum_q q^2 |x_q|^2$ in terms of the capillary modes, $x_q \equiv (1/\sqrt{L}) \int_0^L x(y) e^{-iqy} dy$. From the equipartition theorem, the equilibrium second moment of the Gaussian random variables, $\langle x_q x_{q'} \rangle$ is given by:

$$\langle x_q x_{q'} \rangle = (kT/\tilde{\beta}q^2) \delta_{q',-q}. \quad (2)$$

Using this, it is easy to show that the basic correlation function describing the mean-squared step wandering in the x -direction as a function of the distance y from a given step position:

$$G^l(y) \equiv \langle [x(y) - x(0)]^2 \rangle \quad (3)$$

increases *linearly* with y . Indeed, as the step length L_y goes to infinity, we have the well-known result¹:

$$G^l(y) = kT|y|/\tilde{\beta}. \quad (4)$$

Let us now consider the analogous quantity:

$$G_n(y) \equiv \langle [x_n(y) - x_n(0)]^2 \rangle \quad (5)$$

describing the wandering of a particular step n on a vicinal surface with N_s steps [9,11,12]. As $N_s \rightarrow \infty$, this function becomes independent of n and will be denoted as $G(y)$, since all steps are

¹ See appendix B of Ref. [15] for the finite size effect and see Ref. [16] for a more general discussion of fluctuating interfaces in different dimensions.

equivalent². For small y , and in the absence of very strong direct step–step interactions, the step fluctuations are dominantly controlled by the step stiffness alone. Thus $G(y)$ is linear in y , just like the $G^I(y)$ of the isolated step. However, the isolated step approximation must certainly fail to describe the wandering of the given step on a vicinal surface when $G(y)$ becomes of the order of the average terrace width, or equivalently, when y approaches the *collision length* l_c , defined as the distance y along the average step direction such that $G^I(y)$ is equal to the half width of the average terrace, $w/2$ [5]:

$$l_c(w) \equiv \frac{\tilde{\beta}}{4kT} w^2. \quad (6)$$

Roughly speaking, a step collides with its neighbors³ at y -positions separated by intervals of length l_c .

If the neighboring steps were fixed in place [17], a step that wanders to the neighboring step position must retreat after a collision to avoid overhangs, and the mean-square step displacement would be bounded by the distance between the two neighboring fixed steps. A given step on a real 2D vicinal surface where all steps can fluctuate also tends to rebound after a collision, but now the neighboring step is ‘pushed’ in the opposite direction, providing more space for the original step to wander. Moreover, there exist in-phase modes where the step and many of its neighbors move in the same direction. However, an increasingly large number of neighboring steps are required to move in-phase when $G(y)$ becomes much larger than w . This causes the mean-square step displacement, $G(y)$, to change from linear

behavior at short distances to logarithmic behavior at large length scales [9,11,12].

To see this, let us consider a continuum theory for a 2D vicinal surface with fluctuating steps. Experiments on vicinal surfaces are usually carried out at temperatures well below the roughening temperature of the (low-index) flat surface. However, since the vicinal surface has a non-zero macroscopic slope, it is generally *rough*, with a differentiable free energy as a function of orientation [18,19]. In such a rough phase, the free energy cost for small distortions of long wavelength from the uniform state with step spacing w_a can be written as:

$$H = \frac{1}{2} \sum_q [\tilde{\gamma}_x (w_a q_x)^2 + \tilde{\gamma}_y (a_y q_y)^2] |u_q|^2 \quad (7)$$

in terms of Fourier components of the deviations:

$$u_n(y) \equiv x_n(y) - w_a n \quad (8)$$

from the uniform state:

$$u_q = \frac{1}{\sqrt{N_s N_y}} \sum_{n=1}^{N_s} \sum_{k=1}^{N_y} u_n(y_k) e^{-i(q_x w_a n + q_y y_k)}. \quad (9)$$

Here $y_k = k a_y$ is the y -coordinate of the k th segment of length a_y of the step⁴ and $N_y = L_y/a_y$. Eq. (7) introduces two ‘elastic constants’ or *surface stiffnesses* controlling the energetics of surface distortions: $\tilde{\gamma}_y$, describing the resistance of the step array to bending, and $\tilde{\gamma}_x$, describing the resistance of the surface to changes in the average step spacing. This quadratic model is appropriate only for surfaces with a small slope ($|q u_q| \ll 1$). For perturbations where the small slope approximation breaks down, see Refs. [20–22].

It is easy to determine the relationship between the surface stiffnesses, $\tilde{\gamma}_x$ and $\tilde{\gamma}_y$ and the usual energetic parameters in step models, the step stiffness $\tilde{\beta}$ and the step interaction parameter g by considering two limiting cases of Eq. (7). First, we obtain the relationship between $\tilde{\gamma}_x$ and g by

² In some cases there could exist strong impurities, pinning centers, or other perturbations that could create complicated corrugations normal to the average step direction that might not relax over the course of a typical experiment. In such cases this assumption of step equivalence would break down and our method (as well as the other approaches) could yield inaccurate results.

³ This definition of collision length holds when there are only entropic repulsions. In general, the effective collision length would depend on direct step–step interactions as well as the terrace width and strong step–step repulsions would reduce the collision length.

⁴ One could use a continuum Fourier transform (FT) in y -direction, $x_q = [1/\sqrt{N_s L_y}] \sum_n \int dy u_n(y) e^{-i(q_x w_a n + q_y y)}$, which would give additional powers of N_y/L_y in quantities defined in terms of Fourier components. We choose a discrete FT both in x - and y -directions to avoid the confusion of Fourier components having different dimensions depending on the direction.

considering a limit where the second term in Eq. (7) is negligible. If we allow only $q_y=0$ modes, i.e. if $u_q = u_{q_x,0} \delta_{q_y,0}$, Eq. (7) reduces to a quasi-1D model Hamiltonian describing *straight* steps, and the relationship between $\tilde{\gamma}_x$ and g can easily be obtained. Using the standard quasi-1D step model with pairwise interacting steps [17,23,24], the free energy difference between a non-uniform and a uniform vicinal system for small distortions $u_n \equiv x_n - w_a n$ from the average step spacing w_a is given by:

$$\begin{aligned} H - H_0 &= L_y \sum_n \frac{gh^3}{(u_{n+1} - u_n + w_a)^2} - \frac{gh^3}{(w_a^2)} \\ &\approx \frac{3gh^3 a_y}{w_a^4} \sum_{q_x} 2[1 - \cos(q_x w_a)] |u_{q_x,0}|^2 \\ &\approx \frac{3gh^3 a_y}{w_a^4} \sum_{q_x} (q_x w_a)^2 |u_{q_x,0}|^2 \end{aligned} \quad (10)$$

for small q_x and $|u_{q_x,0}|$. Here L_y is the length of each (straight) step, H_0 is the energy of the uniform vicinal surface, and h is the step height. Comparing this result to Eq. (7) when q_y is set to zero, we find the desired relation:

$$\tilde{\gamma}_x = 6ga_y h^3 / w_a^4. \quad (11)$$

Similarly, the relationship between $\tilde{\gamma}_y$ and $\tilde{\beta}$ can be obtained from a limit in which the second term of Eq. (7) is dominant. Since $\tilde{\gamma}_x$ decreases as $1/w_a^4$, the first term of Eq. (7) can be ignored in the limit $w_a \rightarrow \infty$ and Eq. (7) reduces to:

$$H = \frac{1}{2} \sum_{q_x, q_y} \tilde{\gamma}_y (a_y q_y)^2 |u_q|^2 = \frac{1}{2} \sum_{n=1}^{N_s} \int (\tilde{\gamma}_y a_y) (\partial_y u)^2 dy. \quad (12)$$

In this limit, the system becomes an array of N_s *independent* steps whose fluctuations are controlled by the step stiffness, $\tilde{\beta}$. From Eq. (1), therefore, we have:

$$\tilde{\gamma}_y = \tilde{\beta} / a_y. \quad (13)$$

Strictly speaking, there will be additional contributions to $\tilde{\gamma}_y$ at finite w_a arising from step interactions, since the normal distance between steps also changes as a result of the distortion. However, in

most cases, these corrections are extremely small [22] and we will ignore them here.

The asymptotic behavior of $G(y)$ in Eq. (5) can now be calculated straightforwardly from Eq. (7). For large y , we find the well-known result [9,10,19]:

$$\begin{aligned} G(y) &= \frac{1}{N_s N_y} \sum_{q, q'} \langle u_q u_{q'} \rangle (e^{iq'sy} - 1) (e^{iq'sy} - 1) \\ &\simeq \frac{kT w_a a_y}{4\pi^2 \tilde{\gamma}} \int dq_y dq_x \frac{2[1 - \cos(q_y y)]}{\tilde{\eta} w_a^2 q_x^2 + a_y^2 q_y^2 / \tilde{\eta}} \\ &\simeq \frac{kT}{\pi \tilde{\gamma}} \ln(y/a_y) + \text{const.} \end{aligned} \quad (14)$$

for large y where $\tilde{\gamma} = \sqrt{\tilde{\gamma}_x \tilde{\gamma}_y}$ is the (geometric) mean surface stiffness and $\tilde{\eta} = \sqrt{\tilde{\gamma}_x / \tilde{\gamma}_y}$ measures the anisotropy in the surface stiffnesses. Most vicinal surfaces have $\eta \ll 1$, since $\tilde{\gamma}_y$ depends mainly on the step stiffness $\tilde{\beta}$, while $\tilde{\gamma}_x$ arises mainly from the step-step repulsions, which are relatively weak for typical step spacing. This is consistent with our neglect of the corrections to $\tilde{\gamma}_y$ arising from step repulsions.

Combining this asymptotic large distance behavior with the short distance behavior discussed earlier, we thus expect the mean square step wandering, $G(y)$ to increase linearly for small y but change to logarithmic behavior for large y :

$$G(y) \simeq \begin{cases} C_1(T)y & \text{for } y \ll l_c \\ C_2(T) \log(y) & \text{for } y \gg l_c. \end{cases} \quad (15)$$

By measuring the coefficients, $C_1(T)$ and $C_2(T)$, from step configurations one can in principle obtain the step stiffness $\tilde{\beta}(T)$ and the step interaction parameter $g(T)$ from Eqs. (4), (11) and (14):

$$\begin{aligned} \tilde{\beta}(T) &= kT / C_1(T) \quad g(T) = \tilde{\gamma}_x w_a^4 / 6 = \tilde{\gamma}^2 w_a^4 / (6\tilde{\gamma}_y) \\ &= \frac{1}{6\pi^2} \left[\frac{kT}{C_2(T)/a_x^2} \right]^2 \left[\frac{C_1(T)}{a_x} \right] a_x^2. \end{aligned} \quad (16)$$

Indeed, the step stiffness $\tilde{\beta}(T)$ of several different systems has been determined from the measurement of $C_1(T)$ [6]. However, since $\log(y)$ is a very slowly varying function, to obtain its coefficient $C_2(T)$ accurately one needs the equilibrium con-

figurations of a large sample, and the equilibration time is often very long. There have been a couple of attempts to measure the coefficient of the logarithmic divergence of the step position correlation function [25,26], but it is not clear if the samples reached equilibrium on sufficiently large scales for the analysis to be valid. The distribution of terrace widths on a vicinal surface has also been used to estimate the step interaction parameter [6,14], and recently Einstein and Pierre-Louis [27] have developed improved theoretical expressions that can in principle provide accurate results even for weak elastic interactions, but again a large area of equilibrium configurations is needed for the analysis to be valid.

3. Fluctuation modes of an individual step on a vicinal surface

We now show that g as well as $\tilde{\beta}$ can be obtained by considering the capillary modes of an individual step in the step array and observing the deviation from the prediction of an isolated non-interacting step as a function of the wave vector. Since the capillary mode analysis provides the wavelength dependence of the step–step interaction strength as described below, this method has the advantage of telling the length scale on which a real surface has reached equilibrium in the y (step) direction and may be applied to a surface that has reached only local equilibrium.

Let u_{n,q_y} be the capillary mode of the n th step at a particular wave vector q_y , related by Fourier transform to Eq. (8):

$$u_{n,q_y} = \frac{1}{\sqrt{N_y}} \sum_k u_{n,y_k} e^{-iq_y y_k}. \quad (17)$$

Then, from Eq. (9) we have:

$$u_{n,q_y} = \frac{1}{\sqrt{N_s}} \sum_{q_x} u_{q_x,q_y} e^{iq_x w_a n} \quad (18)$$

and the second moment of the capillary mode at

this particular wave vector is given by:

$$\begin{aligned} C_{q_y} &\equiv \langle u_{n,q_y} u_{n,-q_y} \rangle \\ &= N_s^{-1} \sum_{q_x} \sum_{q'_x} \langle u_{q_x,q_y} u_{q'_x,q_y} \rangle e^{i(q_x + q'_x)w_a n} \\ &\approx \frac{w_a kT}{\pi} \int_{2\pi/L_x}^{\pi/w_a} [\tilde{\gamma}_x(w_a q_x)^2 + \tilde{\gamma}_y(a_y q_y)^2]^{-1} dq_x \\ &\approx \frac{kT}{\pi \tilde{\gamma}_y a_y q_y} \arctan\left(\frac{\pi \tilde{\eta}}{a_y q_y}\right). \end{aligned} \quad (19)$$

As is the case for $G(y)$, C_{q_y} is independent of the step index n since all steps are equivalent. Approximating $\arctan(x)$ by x for $x \ll 1$ and by $\pi(2 + 4/\pi x)^{-1}$ for $x \gg 1$, it is easy to show that:

$$C_{q_y} \approx \begin{cases} \frac{kT}{\tilde{\gamma}_y (a_y q_y)^2} & \text{for } a_y q_y > \pi \tilde{\eta} \\ \frac{kT}{2\tilde{\gamma}_y a_y q_y + (4/\pi^2)\tilde{\gamma}_y (a_y q_y)^2} & \text{for } a_y q_y < \pi \tilde{\eta}. \end{cases} \quad (20)$$

It is instructive to relate these results for the fluctuations of an individual step on a vicinal surface to those of a single *isolated* step as described by a capillary wave Hamiltonian with modified parameter values that take account in some effective way of the presence of the other steps. For our purposes here it is convenient to view Eq. (19) as arising from the fluctuations of a single step with a *wave-vector dependent* ‘equivalent line stiffness’ $\tilde{\beta}_e(q_y)$, which incorporates the effects of step repulsions:

$$H = \frac{1}{2} \sum_q \tilde{\beta}_e(q_y) q_y^2 |u_{q_y}|^2 \quad (21)$$

where:

$$\tilde{\beta}_e(q_y) \equiv \frac{kT}{C_{q_y} a_y^2 q_y^2} \approx \frac{\pi \tilde{\gamma}}{a_y q_y} \left[\arctan\left(\frac{\pi \tilde{\eta}}{a_y q_y}\right) \right]^{-1} \quad (22)$$

$$\approx \begin{cases} \tilde{\gamma}_y & \text{for } a_y q_y > \pi \tilde{\eta} \\ 2\tilde{\gamma}/(a_y q_y) + (4/\pi^2)\tilde{\gamma}_y & \text{for } a_y q_y < \pi \tilde{\eta}. \end{cases} \quad (23)$$

With this choice of $\tilde{\beta}_e$, the isolated step correlation function C_{q_y} will equal that of a step in the array, Eq. (19). As expected, for an isolated step where $\tilde{\eta} = \sqrt{\tilde{\gamma}_x/\tilde{\gamma}_y}$ goes to zero ($w \rightarrow \infty$), $\tilde{\beta}_e(q)$ becomes the q -independent bare step stiffness $\tilde{\gamma}_y$. Note that the equivalent line stiffness, $\tilde{\beta}_e(q)$ diverges as $1/q$ for long wavelength fluctuations. This increasing stiffness causes the mean square step wandering in this equivalent 1D system to diverge logarithmically rather than linearly as it would for a 1D system in zero field and constant stiffness.

To get $\tilde{\gamma}_x$ and $\tilde{\gamma}_y$ (or equivalently $\tilde{\gamma}$ and $\tilde{\eta}$) from experimental data or numerical results, it is advantageous to measure the function $\alpha(q_y) \equiv 1/(a_y q_y C_{q_y})$. When this is plotted versus q_y , one can easily deduce $\tilde{\gamma}_x$ and $\tilde{\gamma}_y$ from the slope and (extrapolated) y -intercept:

$$\alpha(q_y) \approx \frac{\pi\tilde{\gamma}}{kT} \left[\arctan\left(\frac{\pi\tilde{\eta}}{a_y q_y}\right) \right]^{-1} \quad (24)$$

$$\approx \begin{cases} \frac{2\tilde{\gamma}}{kT} + \frac{4\tilde{\gamma}_y}{\pi^2 kT} a_y q_y & \text{for } a_y q_y < \pi\tilde{\eta} \\ \frac{\tilde{\gamma}_y}{kT} a_y q_y & \text{for } a_y q_y > \pi\tilde{\eta}. \end{cases} \quad (25)$$

To test the above prediction, we performed MC simulations on a TSK model and measured $\alpha(q_y)$ for a uniform stable vicinal surface. We used a ‘restricted’ model [28] in which step-kinks larger than one are prohibited, i.e. $E(0)=0$, $E(1)=\epsilon_k$, and $E(n \geq 2)=\infty$. The relationship between the microscopic parameters in the TSK model and those of the mesoscopic step model is well understood. The step stiffness, $\tilde{\beta}$ or $\tilde{\gamma}_y$ can be exactly calculated from the diffusivity of the step [5] and is given by $\tilde{\gamma}_y = kT(1 + \frac{1}{2} e^{\epsilon/kT})/(a_x a_y)$. When there is no direct energetic interaction between steps, such as elastic or magnetic dipole interactions, it is well known that the reduced surface stiffness $\tilde{\gamma} = \pi kT/w_a^2$ [19]. Since the anisotropy of the surface stiffness, $\tilde{\eta}$ is equal to $\sqrt{\tilde{\gamma}_x/\tilde{\gamma}_y} = \tilde{\gamma}/\tilde{\gamma}_y$, we have $\tilde{\eta} = (2\pi a_x a_y/w_a^2)/(2 + e^{\epsilon/kT})$.

In Fig. 1, we plot $\Delta\alpha(q) \equiv \alpha(q_y) - \alpha_0(q_y)$ versus q_y for four different values of w_a . Here α_0 is the α of an isolated step ($w_a = \infty$). The mean surface

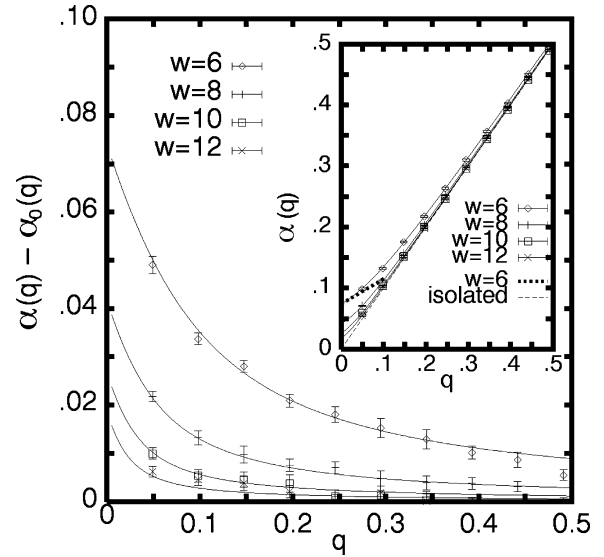


Fig. 1. $\Delta\alpha(q) = \alpha(q) - \alpha_0(q)$ versus q . Data points are from MC simulations on a lattice with 32 steps. Each step is 128 units long and periodic boundary conditions are used. The kink energy $\epsilon_k = 1$. Cases with average terrace width $w_a = 6, 8, 10$ and 12 for wave vectors from $q = 2\pi/L_y = 2\pi/128 \approx 0.05$ to $q = 10(2\pi/L_y) \approx 0.49$ are shown. Solid lines are predictions from Eq. (24). In the inset, $\alpha(q)$ is plotted against q . The thin dashed line represents the case of an isolated step ($w_a = \infty$). Predictions of the asymptotic behavior from Eq. (25) are shown in the $w_a = 6$ case with a thick dotted line.

stiffness $\tilde{\gamma}$ is given by $kTy_0/2$ where y_0 is the extrapolated y -intercept. In the inset, $\alpha(q_y)$ itself⁵, whose slope at large q_y can be used to estimate $\tilde{\gamma}_y$, is plotted against q_y and compared with Eqs. (24) and (25). Here we set the kink energy $\epsilon_k = 1$ and consider the case where there are only entropic repulsions between steps. The data points were obtained from MC simulations on a system with 32 steps. Each step is 128 units long and periodic boundary conditions are imposed. Cases with average terrace widths $w_a = 6, 8, 10$ and 12 are

⁵ $\alpha(q)$ is drawn after the effect of discreteness of a TSK model has been taken into account. Even for a pure 1D system, the quadratic line tension term of the continuum model does not well describe the short wavelength (of order atomic size) fluctuations of a discrete system (1D SOS model or an isolated step in a TSK model) and $\alpha(q)$ deviates from the linear behavior of FD25Eq. (25) for large wave vectors. These deviations are expected to be essentially unchanged for steps on a vicinal surface and hence are estimated using the 1D SOS system and taken into account in the plot.

shown. The collision lengths $l_c = (\tilde{\beta}/4kT)w_a^2 \approx 6w_a^2$ are around 21, 38, 59 and 85 respectively. All data are averaged over 2^{13} MC sweeps after 2^{12} equilibrium sweeps, where a MC sweep consists of $N_s N_y$ attempts to move step segments chosen at random. For long wavelength capillary waves, $q < q_c \equiv \pi/l_c$, deviations from the behavior of an isolated step are clearly noticeable (e.g. for $q < q_c \approx 0.15$ in the $w_a = 6$ case) and these deviations are consistent with the predictions of Eq. (24).

If a surface has reached only local equilibrium but our assumption of the equivalence of all steps in the array remains valid, then information on the capillary modes of an individual step provides an accurate way to estimate the step parameters. To illustrate this, we carried out MC simulations of the above TSK model and measured the mean square step wandering $G(y)$, the distribution $P(w)$ of terrace widths w [6,14], and the amplitudes of the capillary modes in a surface whose long wavelength fluctuation modes have not completely relaxed. We started from a special non-equilibrium initial configuration, an array of straight steps with uniform spacing, and examined how these quantities approach the predicted equilibrium values. The system has 32 steps ($N_s = 32$). Each step is 128 units long ($N_y = 32$) and $w_a = 6$. $G(y)$, $P(w)$, and the deviations of the capillary waves from those of the isolated step $\Delta\alpha$ are measured and averaged at five different time intervals; $\Delta t_1 = 2^7 - 2^8$, $\Delta t_2 = 2^8 - 2^9$, $\Delta t_3 = 2^9 - 2^{10}$, $\Delta t_4 = 2^{10} - 2^{11}$, and $\Delta t_5 = 2^{11} - 2^{12}$ MC sweeps.

Fig. 2a shows $G(y)$ versus y for $\Delta t_1, \dots, \Delta t_5$. We can roughly determine the length scale on which local equilibrium is obtained for a given time interval and see that it increases with time as expected. $G(y)$ of the last interval, the thin solid line, seems to reach the equilibrium value but the system is too small to extract the step-step interaction strength. From Eq. (14), we have:

$$G(y) = C_0 + C_1 \log(y) \quad (26)$$

for large y , with $C_1 = w_a^2/\pi^2$ [19]. The thick dark line is an attempted fit with Eq. (26). We have tried to choose C_0 such that Eq. (26) coincides with the measured $G(y)$ for large y but the fit is very poor. In other words, the system is too small to find the coefficients C_0 and C_1 from the measure-

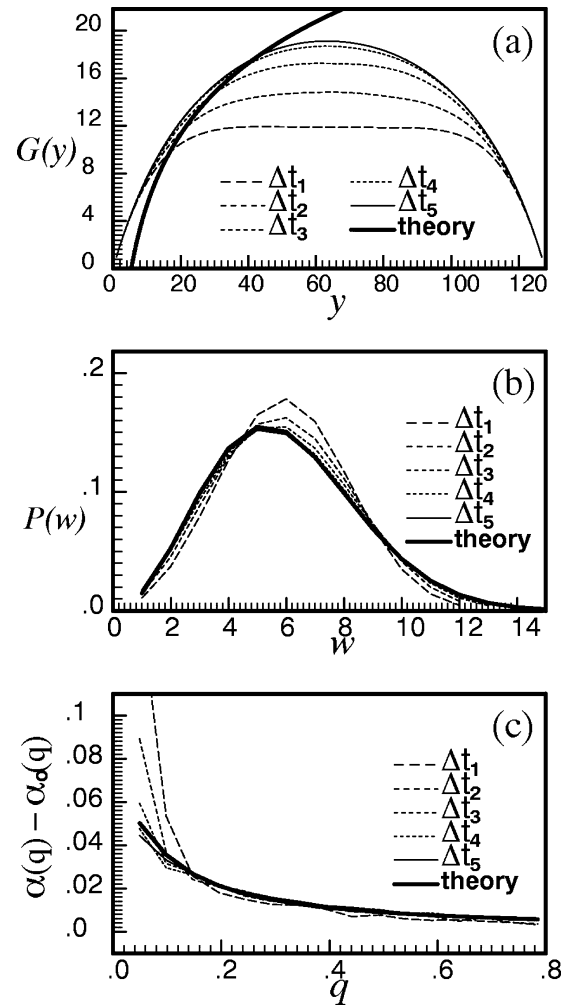


Fig. 2. The mean square step wandering $G(y)$, the distribution $P(w)$ of terrace widths w , and the deviation of the capillary waves from those of the isolated step $\Delta\alpha$ are measured from MC simulations of a TSK model at five different time intervals, $\Delta t_1, \dots, \Delta t_5$.

ment of $G(y)$. To get step-step interactions from $G(y)$, we need a much bigger system, whose equilibration time is correspondingly much longer.

Fig. 2b shows the terrace width distribution $P(w)$. The thick dark line is the theoretical prediction of the equilibrium distribution [14]. $P(w)$ in the last interval, the thin solid line, approaches the equilibrium distribution and nearly coincides with the theoretical prediction. However, it is difficult to tell in advance whether the distribution for a

given time interval and more general step interactions is an equilibrium one or not. For example, $P(w)$ of the first interval (the long dashed line) could be (mis)interpreted as an equilibrium distribution of a system with an additional repulsive energetic interaction between steps, since such step–step repulsions would make the width of the equilibrium distribution narrower.

Fig. 2c shows $\Delta\alpha$ of the capillary waves. Again the thick dark line is the theoretical prediction of an equilibrium system. For the long wavelength [say, $q < 4(2\pi/128) \approx 0.19$] modes, only the measurement from the last interval coincides with the prediction. However, we can tell which wavelength modes are equilibrated for a given time interval. For all five intervals considered here, the short wavelength [say, $q > 6(2\pi/128) \approx 0.29$] modes are equilibrated and coincide with the theoretical prediction.

4. Autocorrelations of the capillary waves and kinetic parameters for step motion

The effects of step–step interactions on the equilibrium fluctuations of capillary modes should also be considered when one tries to deduce the *kinetic* parameters from the autocorrelation function of a capillary mode. Since step motion results from adsorption or emission of atoms at the step edge, the temporal fluctuations in their motion can provide information on the kinetics of adatom movement. Indeed, using a Langevin formalism, Bartelt et al. [7] showed how one can deduce mass-transport modes and kinetic parameters from the autocorrelation function of an *isolated* step. A possible modification of the autocorrelation function due to step–step interactions was considered by Einstein and Khare [29] using a rigid wall approximation [17]. Here, we use the same Langevin analysis but examine how the presence of neighboring *fluctuating* steps in a step array change the wave vector dependence of the autocorrelation function of a particular step on the vicinal surface.

In a linear kinetics approximation, the net mass flux between two regions is proportional to the product of the chemical potential difference and

the linear kinetic coefficient of the mass-transport mode between them. The local step chemical potential $\mu_n(y)$ of the n th step at coarse grained position y is defined as the change in free energy per atom for adding atoms⁶ to the step at position $[x_n(y), y]$:

$$\mu_n(y) \equiv \Omega \frac{\delta H}{\delta x_n(y)} \quad (27)$$

where Ω is the area occupied by an atom and $H(\{x_n(y)\})$ is the free energy functional for step configurations, $\{x_n(y)\}$. Now the equation of step motion (in the linear kinetic theory) can be written as:

$$\partial_t x_n(y) = \sum_{n'=1}^{N_s} \int_0^{L_y} dy' D[x_n(y); x_{n'}(y')] [\mu_n(y) - \mu_{n'}(y')] \quad (28)$$

where $D[x_n(y); x_{n'}(y')]$ is an adatom exchange coefficient matrix. Note that Eq. (28), which provides the velocity of a step in terms of the step configurations only, is obtained by integrating out the role of adatoms on the terrace. Formally, this can be done by solving the diffusion equation on a terrace with the boundary conditions set by the step configurations to obtain the terrace chemical potential profile. If we further integrate out the possible configurations of all other steps for a given configuration of the step n , Eq. (28) reduces to:

$$\partial_t x(y) = \int_0^{L_y} dy' D_1[x(y); x(y')] [\mu(y) - \mu(y')] \quad (29)$$

where we drop the subscript n from x_n and μ_n (all steps are equivalent). Here, $\mu(y)$ is a functional of a single step configuration and is formally defined by $\mu(y) = \Omega \delta H_1[x(y)] / \delta x(y)$ where H_1 is the effective 1D Hamiltonian obtained by integrating out the possible configurations of all other steps. In

⁶ Following Ihle et al. [30] and Khare et al. [31], we consider a vicinal surface in which the terrace behind (left) a step is higher than the terrace in front of (right) the step and the local step position $x_n(y)$ increases when an atom is attached to the step.

general, both the adatom exchange coefficient matrix, D_1 , and the effective step chemical potential, $\mu(y)$, depend on the interactions and are very difficult to calculate. Nevertheless, Eq. (29) can be diagonalized by considering the capillary modes of step motion in many cases [31]. For the analysis of capillary wave motion of steps, it is often convenient to consider Fourier components of the chemical potential, defined by⁷:

$$\mu_q \equiv \frac{1}{\sqrt{L_y}} \int \mu(y) e^{-iqy} dy. \quad (30)$$

If the free energy functional can be represented in terms of capillary modes of step fluctuations, $u_q \equiv (1/\sqrt{L_y}) \int x(y) e^{-iqy} dy$, then μ_q is easily obtained. We have $\mu_q = \Omega \partial_{u_q^*} H(u_q)$ from Eqs. (27) and (30) where u_q^* is the complex conjugate of u_q . For example, μ_q for an isolated step, μ_q^1 , is given by $\mu_q^1 = \Omega \tilde{\beta} q^2 u_q$ since we have $H^1(u_q) = \Sigma_q \frac{1}{2} \tilde{\beta} q^2 |u_q|^2$ from Eq. (1). In general, for small $|u_q|$, the step Hamiltonian can be written as:

$$H = \sum_q \epsilon_q |u_q|^2 \quad (31)$$

in Fourier space for some appropriately chosen ϵ_q , and μ_q is then given by:

$$\mu_q = -2\Omega \epsilon_q u_q. \quad (32)$$

As will be shown below, ϵ_q can be determined from the amplitude of the capillary modes, C_q of Eq. (19). The general form of the adatom exchange coefficient matrix D is not known but in many physically plausible cases, it reduces to a particularly simple form that allows Eq. (29) to be written in Fourier space [31] as:

$$\partial_t u_q = \frac{\Gamma_q}{\Omega kT} \mu_q \quad (33)$$

with an appropriate choice of Γ_q . For example, Eq. (33) is valid for detachment/attachment limited mass transport with $\Gamma_q = \Gamma_+^{s-t} + \Gamma_-^{s-t}$ and for step-edge diffusion limited mass transport with $\Gamma_q = \Gamma^h q^2$ where Γ_{\pm}^{s-t} is the step mobility associated with the adatom exchange between step and terraces and Γ^h is that associated with the adatom

hopping along the step edge. In the surface diffusion limited mass transport case, the standard result for an isolated step [32] is often used to describe fluctuations with wavelength smaller than the average terrace width w_a . Then Eq. (33) holds with $\Gamma_q \sim D_s |q|$ where D_s is the surface diffusion constant [32].

In any case, whenever Eq. (33) holds, the Langevin equation of motion can be written as:

$$\partial_t u_q(t) = -\frac{1}{\tau_q} u_q(t) + \zeta_q(t) \quad (34)$$

where $\tau_q \equiv kT/2\epsilon_q \Gamma_q$ is the relaxation time and the thermal noise ζ_q satisfies the fluctuation–dissipation theorem. The relaxation time τ_q can be obtained by considering the temporal correlations of step-edge fluctuations [33]:

$$C_q(t) = \langle u_q(t) u_q(0) \rangle = C_q(0) e^{-t/\tau_q} \quad (35)$$

where $C_q(0) = \Gamma_q \tau_q = kT/2\epsilon_q$ is the *equilibrium* second moment of the capillary mode. By comparing this prefactor with Eq. (19), we have:

$$\epsilon_q = \frac{\pi}{2} \frac{\tilde{\gamma} a_y q}{\arctan(\pi \tilde{\eta}/a_y q)}. \quad (36)$$

Note that in the limit that $\pi \tilde{\eta}/a_y q$ goes to zero, i.e. when $|q|$ is much larger than $1/l_c$ (which is always the case for an *isolated* step where $1/l_c = 0$), ϵ_q becomes $\frac{1}{2} \tilde{\beta} q^2$ and the relaxation time, $\tau_q = kT/2\epsilon_q \Gamma_q$ is proportional to $|q|^{-2}$, $|q|^{-3}$ and $|q|^{-4}$ for the detachment/attachment, surface diffusion and step-edge diffusion limited mass transport cases respectively, as emphasized by Bartelt et al. [7].

However, for a step on a *vicinal* surface, the relaxation time:

$$\tau_q = \frac{kT}{2\epsilon_q \Gamma_q} = \frac{kT}{\pi} \frac{\arctan(\pi \tilde{\eta}/a_y q)}{\tilde{\gamma} a_y q} \frac{1}{\Gamma_q} \quad (37)$$

does *not* reduce to a simple power of q even for the limiting cases of mass transport where Eq. (33) is valid and the noise amplitude itself satisfies $\Gamma_q \sim q^n$. In general, the effects of step–step interactions on ϵ_q must be taken into account when one deduces the kinetic coefficient, Γ_q from the

⁷ Hereafter, we drop the subscript y and denote q_y as q .

measurement of the relaxation time τ_q through the autocorrelation function of capillary wave modes.

The role of step–step repulsions on capillary wave modes had been previously considered by Einstein and Khare [29]. They considered the displacement of a single step while all other steps remain in their average position (rigid wall approximation [17]) and calculated the leading correction to the step chemical potential. Under this approximation, the displacement of a step, Δx , gives rise to the free energy change $\tilde{\gamma}_x(\Delta x)^2$ and the local step chemical potential becomes $\mu(x) = \beta \partial_y^2 x - 2\tilde{\gamma}_x x$, or in terms of Fourier components, $\mu_q = \epsilon_q u_q = (\beta q^2 + 2\tilde{\gamma}_x) u_q$. This rigid wall approximation is quite accurate for short wavelength fluctuations. Indeed, if we expand Eq. (19) for $a_y q > \pi \tilde{\eta}$, we see that the first order correction of ϵ_q from the isolated step value is constant as predicted by the rigid wall approximation. However, this correction to the relaxation time, τ_q is always numerically very small for short wavelength fluctuations.

On the other hand, the rigid wall assumption is not very accurate for *long wavelength* capillary modes; here the corrections due to step–step interactions are significant. For step fluctuations with $q \lesssim 1/l_c$, the neighboring steps also tend to fluctuate in phase with the original step to reduce the elastic energy in x -direction and $C_q(t)$ of Eq. (35) is quite different from the predictions of the rigid wall approximation. Fig. 3 shows autocorrelations of capillary wave modes, $C_q(t)$ measured from a series of MC simulations of the same TSK model used to determine the equilibrium $\alpha(q)$ in Fig. 1. Metropolis dynamics with a random selection of a step segment for an MC trial movement is used. This dynamic corresponds to the case of attachment/detachment limited mass transport. In Fig. 3a, $C_q(t)$ for two different values of wave vectors, $q_1 = 2(2\pi)/L_y$ and $q_2 = 4(2\pi)/L_y$ are shown in a semi-log plot for systems with two different average terrace widths, $w_a = 6$ and 8. In all cases, data are well fitted with straight lines, indicating an exponential decay of autocorrelations as predicted by Eq. (35). In Fig. 3b, the rescaled autocorrelation, $2\epsilon_q C_q(t)/kT$ is plotted against the rescaled time t/τ_q . All data collapse onto one curve when we use ϵ_q and τ_q given by Eqs. (36) and (37).

Deviations from a single curve are quite noticeable if we rescale the data using ϵ_q and τ_q from either the isolated step approximation or the rigid wall approximation.

5. Capillary wave modes of a step on an unstable surface

In this section, we apply the capillary wave analysis to steps on a *metastable* or *unstable* surface undergoing faceting and show that it can be used to provide a quantitative indication of whether the faceting proceeds by nucleation or by spinodal decomposition [34,35].

An unstable vicinal surface prepared with a single macroscopic orientation will facet into nearby surfaces with stable orientations [36]. For some vicinal surfaces, attractive interactions between the neighboring steps seem to be responsible for the phase separation [37,38]. Recent theoretical work [38–40] showed that a short-ranged attraction between steps can cause a vicinal surface to be unstable even when there are long-ranged repulsive interactions. When the discreteness of the lattice is taken into account, the two competing interactions make steps coalesce into bunches of n steps [40]. A uniform surface can also be made unstable by a sudden change in temperature or chemical composition. For example, a Si(111) surface uniformly vicinal to $[2\bar{1}\bar{1}]$ direction is stable above the 7×7 reconstruction temperature, T_{Re} but becomes unstable below T_{Re} and facets into reconstructed step-free (111) terraces, and more sharply inclined, unreconstructed step-bunched regions. This reconstruction driven faceting, observed in experiments [35], can be understood by assuming that the free energy of fully reconstructed surface, f_r has a lower energy on flat surface ($f_r^0 = f_u^0 - \epsilon_r$) but effectively a higher step creation energy ($\beta_r = \beta_u + \epsilon_s$) than that of the unreconstructed surface, f_u . This leads to an effective short-ranged attractive interaction between steps [41]. Fig. 4a shows two free energy curves, f_u for an unreconstructed surface and f_r for a reconstructed surface, given by [17,42]:

$$f_{u,r}(s) = f_{u,r}^0 + \beta_{u,r}s + g_{u,r}s^3 \quad (38)$$

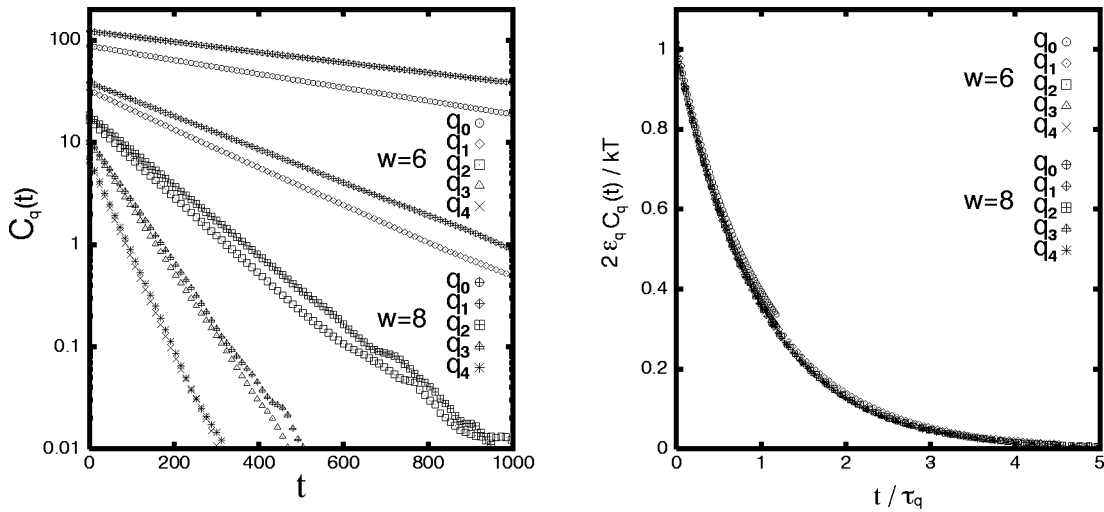


Fig. 3. Autocorrelations of capillary wave modes. Data are from the same MC simulations as in Fig. 1. (a) $C_q(t)$ versus t . Autocorrelations for two different wave vectors, $q_1=2(2\pi)/L_y$ and $q_2=4(2\pi)/L_y$, are shown in a semi-log plot for $w_a=6$ and 8. (b) $2\epsilon_q C_q(t)/kT$ versus t/τ_q with ϵ_q and τ_q given by Eqs. (36) and (37).

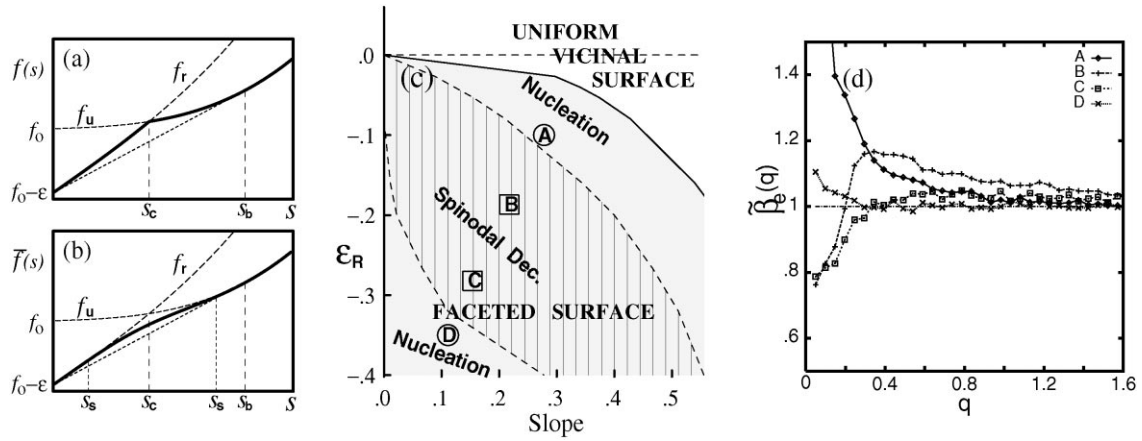


Fig. 4. (a) Free energies for an unreconstructed surface f_u and a reconstructed surface f_r versus slope s . The critical slope, s_c , and the slope of the surface at the step bunches, s_b , are given by $s_c=\epsilon_r/\epsilon_s$ and $s_b=(\epsilon_r/2g)^{1/3}$. (b) A free energy curve is shown that takes account of a distribution of terrace widths. The free-fermion model is used to get the distribution for a given average slope s . The spinodal points, s_s are (numerically) identified by the inflection points of the curve. (c) The phase boundary (solid line) between two equilibrium states, the uniform coexistence state (white region) and the phase separated state (shaded region) are given by $s=s_b(\epsilon_r)$. The spinodal lines (dotted lines) are obtained by connecting the spinodal points calculated for several different values of ϵ_r . Two spinodal lines separate the spinodal decomposition regime (hatched with vertical lines) from the nucleation regime. (d) $\hat{\beta}_c(q)$ of the systems quenched to four different points in the two-phase region, A, B, C, and D in (c). In cases A and D, $\hat{\beta}_c(q)$ is larger than $\hat{\gamma}_y$ while it is smaller than $\hat{\gamma}_y$ at long wavelengths in cases B and C.

where s is the slope of the vicinal surface from the low-index flat surface and f^0 , β and g have the usual meaning of surface free energy per unit area of flat surface, unit length step creation energy for

an isolated step and the step–step interaction parameter [43]. For simplicity, we assume the same g for both surfaces and set $g_r=g_u=g$. The two curves cross each other at the *critical slope*

$s_c = \epsilon_r/\epsilon_s$ and f_r is smaller than f_u only for $s < s_c$. The lower envelope of the thick curve is the true equilibrium free energy that describes the final phase separated state of the system. It predicts the phase separation of any vicinal surface with slope $s < s_b \equiv (\epsilon_r/2g)^{1/3}$ to a flat facet ($s=0$) and the step-bunched surface with slope s_b .

To describe the kinetics of phase separation in a linear kinetics approach, one needs to consider the (quasi-equilibrium) free energy of the *initial* state in the process of the phase separation. The thick curve in Fig. 4a, given by $f(s) = f_u(s) - (1 - s/s_c)\epsilon_r\theta(s - s_c)$, represents the free energy of a hypothetical system in which all terraces are completely reconstructed [unreconstructed] when the average slope s is less [greater] than s_c [35,44]. If this combined curve accurately represented the free energy of the system that was quenched into the phase separation regime, faceting would always occur through nucleation since the free energy curve loses its local convexity only at s_c [45].

It has been speculated that the breakdown of the local convexity, needed for spinodal decomposition [34,35,46,47] may come from a coupling between the kinetics of reconstruction and of step motion [35]. However, a limit that may better describe experiment is when the two kinetic processes are effectively *uncoupled*, because reconstruction occurs on sufficiently wide terraces much faster than the typical time scale for step motion. If we take the limit of infinitely fast reconstruction kinetics, we arrive at the simple two-state *critical width model* [44,48], in which each terrace is either reconstructed or unreconstructed, depending on whether its local width is larger than w_c . This minimal model has several limitations when applied to the faceting dynamics of real materials, as mentioned in Ref. [44]. However, it allows us to illustrate very simply how to construct a kinetic phase diagram analytically for a given model and to show how the analysis of the step capillary waves, considered in Section 3, can be used to distinguish between the two kinetic regimes.

We first show that by taking into account the *distribution* of terrace widths for given average slope, s [45], we can arrive at an initial free energy curve with a smoothly varying *concave* region even for this two-state critical width model, as shown

in Fig. 4b. Fig. 4c gives a kinetic phase diagram for the critical width model. To obtain this diagram, we first calculated the relative number of terraces whose width is larger than w_c and their relative area, for given average slope s and critical width $w_c = \epsilon_s/\epsilon_r$, using the predicted terrace width distribution from the free-fermion model [14,23]. In accord with the critical width model, we assume that reconstruction takes place instantly on all terraces wider than w_c , and take account of the resulting free energy change to determine the spontaneous free energy, $\tilde{f}(s)$, of the initial quenched uniform vicinal surface with average slope, s . The smooth thick line curve in Fig. 4b shows this modified free energy, $\tilde{f}(s)$ for a particular value of ϵ_s/ϵ_r . Then the spinodal points, s_s are (numerically) identified by the inflection points of the curve. The spinodal lines, the dotted lines in the phase diagram of Fig. 4c, are obtained by connecting the above spinodal points calculated for several different value of ϵ_r (we used the same ϵ_s for all cases). The uniform coexistence state (white region) and the phase separated state (shaded region) are separated by a phase boundary (solid line) given by $s = s_b(\epsilon_r) = (\epsilon_r/2g)^{1/3}$, since the uniform vicinal surface (with 1×1 surface structure) has the lowest free energy for $s > s_b$, as can be seen in Fig. 4a and b. Two spinodal lines (dotted lines) in the shaded region separate the spinodal decomposition regime (hatched with vertical lines) from the nucleation regime.

A series of MC simulations of the TSK model (using the critical width model to describe reconstruction) were performed. The equivalent line stiffness, $\tilde{\beta}_e(q)$ of Eq. (22) was measured to analyze the effects of the neighboring steps on the fluctuations of a given step on a surface undergoing the faceting process. On a stable surface, step-step repulsions from the neighboring steps inhibit the fluctuation of the given step and cause $\tilde{\beta}_e(q)$ always to be *larger* than the step stiffness, $\tilde{\gamma}_s$, which is the $\tilde{\beta}_e(q)$ for an isolated step. When the system is quenched to the *nucleation* regime, the surface is metastable, and hence we expect the presence of neighboring steps will still increase $\tilde{\beta}_e(q)$. On the other hand, in the *spinodal* regime, where the uniform step configuration is *unstable* to spontaneous decomposition everywhere, we expect that

the step should fluctuate more than an isolated step and hence that $\tilde{\beta}_e(q)$ would become *smaller* than $\tilde{\gamma}_y$.

Fig. 4d shows $\tilde{\beta}_e(q)$ of systems that were quenched from above T_{re} to four different points in the low-temperature two-phase region. Two, A and D, are in the nucleation regime and the other two, B and C, are in the spinodal decomposition regime. We first prepared a configuration above T_{re} without any reconstruction on the terraces ($\epsilon_r = \epsilon_s = 0$). As in Section 2, the step kink energy for the high temperature configurations was set to $\epsilon_k = 1$, in units of the temperature of the system. We then turned on the reconstruction using four different values of ϵ_r as indicated in Fig. 4c. We use the same value of ϵ_s that we assumed for the calculation of the phase diagram. The same value of ϵ_k is also used in all four cases⁸. Note that the phase diagram of Fig. 4c is independent of the kink energy since the distribution of terrace widths in the free-fermion model does not depend on it [14].

Equivalent line stiffnesses, $\tilde{\beta}_e(q)$ shown in Fig. 4d, are obtained from the first few hundred MC configurations just after the quench, averaging over millions of independent MC runs with different initial step configurations. The step stiffness, $\tilde{\gamma}_y$, which is equal to $\tilde{\beta}_e(q)$ of the isolated step, is also shown for comparison. For cases A and D, $\tilde{\beta}_e(q)$ is *larger* than $\tilde{\gamma}_y$ and the increments are more significant at long wavelengths, indicating that the steps are on a (meta)stable surface. On the other hand, for cases B and C, $\tilde{\beta}_e(q)$ at long wavelengths is *smaller* than $\tilde{\gamma}_y$, indicating the large fluctuations in the step configurations characteristic of steps on an unstable surface. [The increase of $\tilde{\beta}_e(q)$ at short wavelengths in case B is due to the steps in step bunches⁹, which already formed in the initial few hundred MCS.] These results indicate that points A and D are in the nucleation regime while B and C are in the spinodal decomposition regime, which is consistent with the predic-

⁸ We could also use different values of the kink energies but this changes the collision length, l_c , and somewhat complicates the analysis.

⁹ For fully faceted surface, most steps are in the step bunches and $\tilde{\beta}_e(q)$ becomes the $\tilde{\beta}_e(q)$ of the stable uniform surface with $s = s_b$.

tions of the phase diagram in Fig. 4c. To construct a detailed kinetic phase diagram for faceting of real surfaces, we should consider more realistic models for the surface properties. However, we believe the qualitative picture of the phase diagram constructed here is valid for most reconstruction-driven faceting systems.

In summary, we have shown that the capillary wave analysis of fluctuations of an individual step, both on stable and unstable surfaces, can provide important information about the surface structure and dynamics, and in many cases determine the length scale on which the surface has reached equilibrium. We believe that the analysis presented in this paper can be applied to real step images of the surface and can be an efficient way to obtain accurate values for the key parameters in the description of faceting dynamics.

Acknowledgements

We are grateful to D.-J. Liu and E.D. Williams for helpful discussions. This work was supported by the NSF-MRSEC grant DMR96-3252 and the KRF-IDR grant B00001.

References

- [1] E.D. Williams, N.C. Bartelt, *Science* 251 (1991) 393.
- [2] H.-C. Jeong, E.D. Williams, *Surf. Sci. Rep.* 252 (1999) 5.
- [3] F.P. Buff, R.A. Lovett, F.H. Stillinger, *Phys. Rev. Lett.* 15 (1965) 621.
- [4] J.D. Weeks, *J. Chem. Phys.* 67 (1977) 3106.
- [5] N.C. Bartelt, T.L. Einstein, E.D. Williams, *Surf. Sci.* 276 (1992) 308.
- [6] C. Alfonso, J.M. Bermond, J.C. Heyraud, J.J. Métois, *Surf. Sci.* 262 (1992) 371.
- [7] N.C. Bartelt, T.L. Einstein, E.D. Williams, *Surf. Sci.* 312 (1994) 411.
- [8] E.D. Williams, *Surf. Sci.* 299/300 (1994) 502.
- [9] T. Yamamoto, Y. Akutsu, N. Akutsu, *J. Phys. Soc. Jpn.* 63 (1994) 915.
- [10] L. Barbier, L. Masson, J. Cousty, B. Salanon, *Surf. Sci.* 345 (1996) 197.
- [11] Y. Akutsu, N. Akutsu, T. Yamamoto, *J. Phys. Soc. Jpn.* 63 (1994) 2032.
- [12] K. Sudoh, T. Yoshinobu, H. Iwasaki, N. Akutsh, Y. Akutsu, T. Yamamoto, *J. Phys. Soc. Jpn.* 65 (1996) 988.

- [13] X.-S. Wang, J.L. Goldberg, N.C. Bartelt, T.L. Einstein, E.D. Williams, *Phys. Rev. Lett.* 65 (1990) 2430.
- [14] B. Joós, T.L. Einstein, N.C. Bartelt, *Phys. Rev. B* 43 (1991) 8153.
- [15] S. Kodiyalam, K.E. Khor, N.C. Bartelt, E.D. Williams, S.D. Sarma, *Phys. Rev. B* 51 (1995) 5200.
- [16] M.E. Fisher, D.S. Fisher, *Phys. Rev. B* 25 (1982) 3192.
- [17] E.E. Gruber, W.W. Mullins, *J. Phys. Chem. Solids* 28 (1967) 875.
- [18] S.T. Chui, J.D. Weeks, *Phys. Rev. B* 14 (1976) 4978.
- [19] J. Villain, D.R. Grempel, J. Lapujoulade, *J. Phys. F: Met. Phys.* 15 (1985) 809.
- [20] D. Wallace, R. Zia, *Phys. Rev. Lett.* 43 (1979) 808.
- [21] D.A. Huse, W. van Saarloos, J.D. Weeks, *Phys. Rev. B* 32 (1985) 233.
- [22] H.P. Bonzel, W.W. Mullins, *Surf. Sci.* 350 (1996) 285.
- [23] C. Jayaprakash, C. Rottman, W.F. Saam, *Phys. Rev. B* 30 (1984) 6549.
- [24] A. Rettori, J. Villain, *J. Phys. (Fr.)* 49 (1988) 257.
- [25] J.C. Heyraud, J.M. Bermond, C. Alfonso, J. Métois, *J. Phys. I (Fr.)* 5 (1995) 443.
- [26] J.L. Goldberg, X.-S. Wang, N.C. Bartelt, E.D. Williams, *Surf. Sci.* 249 (1991) L285.
- [27] T.L. Einstein, O. Pierre-Louis, unpublished results.
- [28] H. van Beijeren, *Phys. Rev. Lett.* 38 (1977) 993.
- [29] T.L. Einstein, S.V. Khare, in: P.M. Duxbury, T. Pence (Eds.), *Dynamics of Crystal Surfaces and Interfaces*, Plenum Press, New York, 1997, p. 83.
- [30] T. Ihle, C. Misbah, O. Pierre-Louis, *Phys. Rev. B* 58 (1998) 2289.
- [31] S.V. Khare, T.L. Einstein, *Phys. Rev. B* 57 (1998) 4782.
- [32] W.W. Mullins, in: W.D. Robertson, N.A. Gjostein (Eds.), *Metal Surfaces*, American Society of Metals, Metals Park, OH, 1962, p. 17.
- [33] J. Villain, *J. Phys. I* 1 (1991) 19.
- [34] J.W. Cahn, *Trans. Met. Soc. AIME* 242 (1968) 167.
- [35] R.J. Phaneuf, N.C. Bartelt, E.D. Williams, W. Świąch, E. Bauer, *Phys. Rev. Lett.* 71 (1993) 2284.
- [36] C. Herring, *Phys. Rev.* 82 (1951) 87.
- [37] S. Song, S.G.J. Mochrie, *Phys. Rev. Lett.* 73 (1994) 995.
- [38] M. Lässig, *Phys. Rev. Lett.* 77 (1996) 526.
- [39] S.M. Bhattacharjee, *Phys. Rev. Lett.* 76 (1996) 4568.
- [40] V.B. Shenoy, S. Zhang, W. Saam, *Phys. Rev. Lett.* 81 (1998) 3475.
- [41] D.-J. Liu, J.D. Weeks, *Phys. Rev. Lett.* 79 (1997) 1694.
- [42] H.-C. Jeong, J.D. Weeks, *Phys. Rev. Lett.* 75 (1995) 4456.
- [43] H.-C. Jeong, J.D. Weeks, *Phys. Rev. B* 57 (1998) 3949.
- [44] J.D. Weeks, D.-J. Liu, H.-C. Jeong, in: P. Duxbury, T. Pence (Eds.), *Dynamics of Crystal Surfaces and Interfaces*, Plenum Press, New York, 1997, p. 199.
- [45] H.C. Jeong, J.D. Weeks, *Scan. Microsc.*, in press.
- [46] J. Stewart, N. Goldenfeld, *Phys. Rev. A* 46 (1992) 6505.
- [47] F. Liu, H. Metiu, *Phys. Rev. B* 48 (1993) 5808.
- [48] D.-J. Liu, J.D. Weeks, M.D. Johnson, E.D. Williams, *Phys. Rev. B* 55 (1997) 7653.